**Interdecadal Variability of the Eastward Current in the South China Sea Associated with the Summer Asian Monsoon**

Guihua Wang[1] Chunzai Wang[2] Rui Xin Huang[3]

1, State Key Laboratory of Satellite Ocean Environment Dynamics, Second institute of Oceanography, SOA, Hangzhou, China

2, Physical Oceanography Division, NOAA/Atlantic Oceanographic and Meteorological Laboratory, Miami, Florida, USA

3, Woods Hole Oceanographic Institution, Woods Hole, Massachusetts, USA

Submitted to *Journal Of Climate (revised)*

June 2010

Corresponding email: guihua_wanggh@yahoo.com.cn

**ABSTRACT:** Based on Simple Ocean Data Assimilation (SODA) dataset and three types of Sverdrup streamfunction, an interdecadal variability of the eastward current in the middle South China Sea (SCS) during summer is identified. Both the pattern and strength of the summer Asian monsoon wind stress curl over the SCS contribute to the interdecadal variability of this current. From 1960 to 1979, the monsoon intensified and the zero wind stress curl line shifted southward. Both the core of positive wind stress curl in the northern SCS and the negative curl in the southern SCS moved southward and thus induced a southward shift of both the southern anticyclonic and northern cyclonic gyres, resulting in a southward displacement of the eastward current associated with these two gyres. In the mean time, the southern (northern) SCS anticyclonic (cyclonic) ocean gyre weakened (strengthened), and therefore also induced the southward of the eastward current near the intergyre boundary. In contrast, the eastward current shifted northward from 1980 to 1998 because the monsoon relaxed and the zero wind stress curl line shifted northward. After 1998, the eastward jet moved southward again as the zero wind stress curl line shifted southward and the SCS monsoon strengthened. The eastward current identified from the baroclinic streamfunction moved about $1.7^{o}$ more southward than that from the barotropic streamfunction, indicating that the meridional position of the eastward current is depth-dependent.

## 1. Introduction

The South China Sea (SCS) is the largest semi-enclosed marginal sea in the tropical western Pacific. Its upper layer circulation is driven mainly by the Asian monsoon. The monsoon-driven circulation shows a large seasonality, having a relatively short thermocline adjustment time of 1 to 4 months (Liu et al. 2001). Forced by the southwesterly monsoon wind in summer, the circulation in the basin consists of a cyclonic gyre north of about 12°N and a strong anticyclonic gyre south of 12°N. Thus, there is an eastward current veering off central Vietnam between these two gyres (Liu et al. 2001). The large scale cyclonic gyre in northern SCS, the anticyclonic gyre in southern SCS and the accompanying eastward current between these two gyres are clearly evident in the summer mean thermocline depth characterized by 20$^{o}$C isotherm (Figure 1), which is derived from Simple Ocean Data Assimilation (SODA) data(Carton and Giese 2008). Figure 2 also shows the vertical structure of the zonal current along 113$^{o}$E derived from the SODA reanalysis data. Near the surface, the eastward current is confined within the latitude band between 9$^{o}$N-15$^{o}$N. At about 130m, the eastward current is present along 10$^{o}$N-13$^{o}$N. Associated with the summer eastward jet, there is often a dipole-like eddy structure, consisting of an anticyclonic eddy south of the jet and a cyclonic eddy north of it (Metzger et al. 2001, Wang et al. 2006).

Xu et al. (1982) first identified the eastward jet from the climatologic map of dynamic height. In the past decade, the eastward jet was studied using different datasets, including satellite sea surface temperature, sea surface height and chlorophyll signature (Kuo et al. 2000; Liu et al. 2002; Xie et al. 2003). The eastward jet is also found to exist from the surface to a depth of more than 400m in temperature, salinity and current profiler data (Fang et al. 2002). The eastward jet has a large seasonality: starting to appear in May or June, peaking in August or September, and disappearing in October (Metzger and Hurlbut, 1996; Kuo et al. 2000; Xie et al. 2003; Wang et al. 2006). Due to advection by the eastward jet, the cold filament is located off central Vietnam and shows significant interannual variability. In 1998 when the 97/98 El Niño was in the decay phase, the cold filament and mid-summer cooling was weak, suggesting an interannual variability of the eastward jet (Wang, 2004). As a major forcing of SCS circulation, the Asian monsoon contributes to the seasonal and interannual variability of the eastward jet (Xie et al. 2003; Wang 2004). The eastward jet is primarily governed by the wind-driven circulation in the basin interior (Wang et al., 2006; Bayler and Liu, 2008); in addition, it may be partly regulated by the coastal circulation (Gan and Qu, 2008).

The Asian monsoon over the SCS (hereafter, the SCS monsoon) also shows a strong interdecadal variability, which can be clearly seen in the distribution and strength of precipitation over the east China and the large-scale atmospheric circulation (Hu 1997). Wang et al. (2009) suggested that the interdecadal variability of the SCS summer monsoon is closely associated with ENSO. Before the late 1970s, the SCS summer monsoon was primarily influenced by the developing phase of ENSO, while after the late 1970s it was mainly influenced by the decaying phase of ENSO. Since the monsoon is a major forcing of SCS ocean circulation, a natural question is whether the oceanic eastward jet off central Vietnam in summer also varies on interdecadal time scale. This paper is focused on the eastward jet in the SCS, including its interdecadal variability and the causes.

## 2. Simple diagnostic models

Given the time-dependent wind stress in the basin, a barotropic streamfunction can be defined in terms of a time-delayed integral of the wind stress curl, as shown by Qiu and Lukas (1996), Liu et al. (2001) and Huang and Liu (2010):

$$\psi_{bt}(x,y,t_0) = -\frac{f}{\beta}\int_x^{x_e} w_e\left(x',y,t_0-\frac{x'}{C(y)}\right)dx' + \frac{1}{f\rho_0}\int_x^{x_e}\tau^x dx \qquad (1)$$

where x and y are the zonal and meridional coordinates, $t_o$ is a given time we chose. f is the Coriolis parameter, $\beta$ is the meridional gradient of planetary vorticity, $x_e$ is the ocean eastern boundary, $w_e$ is the Ekman pumping velocity calculated from wind stress $w_e = \frac{\partial}{\partial x}(\frac{\tau^y}{\rho f}) - \frac{\partial}{\partial y}\left(\frac{\tau^x}{\rho f}\right)$, $\rho_0$ is the reference density of seawater, and $\tau^x$ and $\tau^y$ are the zonal and meridional components of the surface wind stress. In Eq. (1), $C(y)$ is the speed of long Rossby waves obtained by solving the linearized vertical eigenvalue problem with climatology temperature and salinity data (Cai et al. 2008), and x'/c(y) is the time delay due to the propagation of Rossby wave.

The right hand side of Eq. (1) consists of two terms: the Ekman pumping term and the term associated with the Ekman transport due to zonal wind stress. If both terms are included, this streamfunction represents the time dependent barotropic transport streamfunction for flow integrated over the entire water column. Equation (1) is called the time-dependent barotropic Sverdrup balance.

If we omit the second term and consider the first term only, Eq. (1) is reduced to

$$\psi_{bc}(x,y,t_0) = -\frac{f}{\beta}\int_x^{x_e} w_e\left(x',y,t_0-\frac{x'}{C(y)}\right)dx'. \tag{2}$$

Equation (2) is called the time dependent upper-ocean baroclinic Sverdrup balance and the streamfunction is called the time dependent baroclinic streamfunction. Note that "baroclinic" used here means the circulation below the Ekman layer; thus, it is different from the traditional definition. In fact, this baroclinic streamfunction represents the geostrophic flow below the Ekman layer.

If we omit the delay time correction in the first term of Eq. (1) and assume that the ocean is in near-equilibrium with the wind forcing, Eq. (1) is reduced to the following form

$$\psi_{bt}^{nodelay}(x,y,t_0) = -\frac{f}{\beta}\int_x^{x_e} w_e\left(x',y,t_0\right)dx' + \frac{1}{f\rho_0}\int_x^{x_e}\tau^x dx \tag{3}$$

This streamfunction without considering the effect of time delayed Rossby wave is called the time-independent barotropic streamfunction and the corresponding transport is called the time-independent barotropic transport.

## 3. Data and SCS monsoon indices

The wind data is the recent updated data provided by the European Center for Medium Range Weather Forecasts ERA-40 reanalysis spanning the period from 1958 to 2008. The wind field is used to calculate the time evolution of the streamfunction defined in Eqs. (1), (2) and (3), and maps of the summer season circulation are shown in Figure 3b and Figure 4. The wind data was also used in generating the SODA reanalysis product through the Parallel Ocean Program (Carton and Giese 2008).

Large scale circulation in the upper ocean of SCS is dominated by wind forcing. The essential part of the SCS monsoon wind variability can be represented in terms of its vorticity. As Wang et al. (2009) showed, the meridional gradient of zonal wind can be used as a good measure for SCS monsoon variations from intraseasonal to interdecadal timescales. They proposed a SCS monsoon index (SCSMI) which is defined as the zonal wind difference between a north box and a south box over the SCS at 850-hPa. Because the upper level circulation in SCS is primarily regulated by wind stress curl, which can be further reduced to an index related to the meridional gradient of zonal wind stress, we introduce a modified SCSMI:

$$SCSMI= \tau^x \text{ (5.25-10.25}^o\text{N, 110-120}^o\text{E) - } \tau^x \text{ (17.25-22.25}^o\text{N, 110}^o\text{E-120}^o\text{E)}, \quad (4)$$

where $\tau^x$ is the surface zonal wind stress. For a better understanding of the physics in Eq. (4), we rearrange Eq. (4) as follows:

$$SCSMI= [\tau^x \text{ (5.25-10.25}^o\text{N, 110-120}^o\text{E)- } \tau^x \text{ (around 12}^o\text{N, 110-120}^o\text{E)]}$$

$$+[\tau^x \text{ (around 12}^o\text{N, 110-120}^o\text{E)- } \tau^x \text{ (17.25-22.25}^o\text{N, 110}^o\text{E-120}^o\text{E) ]} \quad (5)$$

Now the physics is clear: the first and second square brackets represent the wind stress curl in the southern and northern SCS, respectively. If wind stress curl in the southern SCS is smaller (more negative) and/or the wind stress curl in the northern SCS is smaller (less positive), the SCSMI is smaller. The corresponding changes in the ocean include: strengthening of the southern SCS anticyclonic gyre and weakening of the northern SCS cyclonic gyre, and thus a northward shift of the eastward current between these two gyres. On the other hand, if the wind stress curl in the southern SCS is larger (less negative) and/or the wind stress curl in the northern SCS is larger (more positive), the SCSMI is larger, then the southern SCS anticyclonic circulation is weakened and/or the northern SCS cyclonic circulation is strengthened, and thus the eastward current between these two gyres moves southward. The SCSMI proposed above can serve as a good index for the wind-driven SCS ocean circulation and the north-south shift of the eastward current. Although the index is slightly different from that defined by Wang et al. (2009), the variability of the two indices is similar.

## 4. Results

### a) Wind forcing and eastward current

The SCS southwesterly monsoon usually starts in April or May. It is further developed from June to August and retreated in September. Associated with this wind distribution, the summer wind stress curl is positive in the northwestern SCS and negative in the southeastern SCS during the summer months (Figure 3a). Driven by the wind stress curl, a double gyre circulation, with a cyclonic gyre north of about $12^{o}$N and an anticyclonic gyre south of $12^{o}$N, starts to develop from May (Wang et al., 2006). The double gyres are further developed in June and July, and matured in August. The oceanic eastward jet between these two gyres also intensifies as summer progresses. Figure 3b demonstrates the summer mean wind-driven Sverdrup ocean circulation, by assuming that the ocean is in near-equilibrium with monthly monsoon forcing.

A more accurate streamfunction in the SCS, the linear time-dependent Sverdrup theory (Eq. 1), can be used to include the effect of thermocline adjustment for the time-dependent wind stress. With speed on the order of 10-40 cm/s, the planetary waves cross the SCS in 1 to 5 months (Cai et al. 2008). Figure 4a shows the summer mean streamfunction including the thermocline adjustment. Although transportation patterns shown in Figures 4a and 4b share similar features, the difference in magnitude in the northern SCS is prominent. The cyclonic gyre in Fig. 4a weakens from 13$^{o}$N to 16$^{o}$N; while it intensifies north of 16$^{o}$N. Such a difference may result from the wind stress curls (positive wind stress curl in northwestern Luzon Island and negative wind stress curl in west of Manila Bay) in the northeasterly winter monsoon season (Wang et al., 2008). The comparison between these two solutions demonstrates that the winter wind can affect the summer circulation in northern SCS. The difference in magnitude south of 13$^{o}$N is relatively small because the thermocline adjustment time at this latitude is about 1 month and thus the ocean is nearly in equilibrium with the monthly wind forcing. It is interesting to note that the positions of the eastward flow in Figures 3b and 4a, as identified by the zero streamfunction contours, are almost identical.

To examine the effect of Ekman transport on the latitudinal position of the eastward flow, Figure 4b shows the upper-ocean baroclinic streamfunction. Although the pattern and magnitude of baroclinic streamfunction is similar to those of the barotropic streamfunction in Figure 3a, the latitude of the eastward flow is significantly alternated by including the Ekman transport. The eastward flow in baroclinic streamfunction (red line in Figure 4b) is about 1-3$^{o}$ more southward than that obtained from the barotropic streamfunction (green line in Figures 4a and 4b). This indicates that the eastward current is depth-dependent.

Comparing these three types of theoretic Sverdrup streamfunction (Figure 3b, Figure 4a and Figure 4b) with the SODA reanalysis (Figure 1) suggests that the Sverdrup balance proves a good representation of the oceanic transport pattern in SCS. Thus, it is possible to use the Sverdrup theory to examine the SCS circulation in summer season and infer the corresponding variability of the eastward current.

**b) Interdecadal variability of the eastward current**

Now we focus on the north-south migration of the eastward jet. We define $T_b$ as the latitude where the depth of 20$^{o}$C is 100m along the 113$^{o}$E section, as inferred from SODA data. The solid dot in Figure 1 denotes the mean position of $T_b$ in summer. Figure 5 shows the time series of $T_b$ from the SODA data during 1960-2007. It is clear that the time series contains interdecadal signals. Before 1980, the eastward current gradually shifted to the south with time, from 18.0$^{o}$N around 1962 to 12.2$^{o}$N around 1979. After 1980, the eastward current showed a northward shift with time, reaching the northernmost position (around 18.0$^{o}$N) in 1998. The eastward jet then moved southward again after 1998. Figure 5 also shows the results obtained by a 15-year-low-pass Butterwort filter, which can separate the interdecadal signals from other unwanted signals. The low pass filtered results also show that the eastward jet moved southward, northward and southward during the periods of 1960-1979, 1980-1998 and 1999-2007, respectively. The trend rates in the three periods are listed in Table 1.

The three types of Sverdrup model can be used to study the interdecadal variability of the eastward currents, and Figure 6 shows the summer ensemble mean streamfunction derived from the three models over the periods of 1960-1979, 1980-1998 and 1998-2007. The patterns of these three types of streamfunction for each period are very similar, except the eastward current over the periods of 1960-1979 is slightly more northward than the other two periods. Therefore, these three types of Sverdrup balance model can be used as useful diagnosis tools. Actually, the pattern of these streamfunction is relative stable because the wind stress curl pattern is strongly regulated by flow over steep topography associated with the mountain on the east coast of Vietnam (Xie et al., 2003).

As the next step, these three types of Sverdrup streamfunction were used to examine the interdecadal variability of the eastward current. We define $Y_b$ as the latitude where the time-independent barotropic streamfunction is zero along the 113$^o$E section. The solid dot in Figure 3b denotes the mean position of $Y_b$ (13.76°N) in summer by assuming that the ocean is in near-equilibrium with monthly monsoon forcing. For the cases shown in Figures 4a and 4b, the eastward currents are located at 13.74$^o$N and 11.84$^o$N for the time-dependent mean barotropic and baroclinic streamfunctions, respectively.

Figure 7a shows three time series of $Y_b$ from the time-independent barotropic Sverdrup model, the time-dependent barotropic Sverdrup model and the time-dependent baroclinic Sverdrup model during 1960-2007. Generally, these three time series have good correlation with the time series of $T_b$ from the SODA data. The correlation coefficients are 0.48, 0.56 and 0.52 between $T_b$ and $Y_b$ derived from the time-independent barotropic Sverdrup model, the time-dependent barotropic Sverdrup model and the time-dependent baroclinic Sverdrup model respectively. All of them are significant at the 95% confidence level. These three time series also include noticeable interdecadal signals. Before 1980, the eastward current shifted to the south with time, from 16.5$^o$N around 1965 to 11$^o$N around 1979. After 1980, the eastward current moved northward with time, reaching the northernmost position in 1998. The eastward jet then moved southward again after 1998. The trend rates in three periods for the three time series are listed in Table 1. All the trends in Table 1 are statistically significant at the 95% level. The trend rates for the time-dependent baroclinic Sverdrup model, regardless of upward or downward, are larger than those for the time-dependent barotropic Sverdrup model.

The time series of $Y_b$ of the eastward flow derived from the time-independent barotropic Sverdrup model and the time-dependent barotropic Sverdrup model are almost the same (Figure 7a). Both the time series (Figure 7a) and the spatial patterns (Figure 3b and Figure4a) demonstrate that the winter wind may not affect the eastward current position in summer, while it can affect the northern SCS circulation in summer. Again, the time series of $Y_b$ for the eastward flow derived from the time-dependent baroclinic Sverdrup model shows that latitude $Y_b$ is strongly affected by Ekman transport, and located about 0-6.6$^o$ (mean value is 1.7$^o$) farther southward than that obtained from the barotropic streamfunction. Again, this indicates that the latitudinal position of the eastward current is depth-dependent. The largest difference is 6.6°N in 1964 while there is no difference in 1966 and 1999 (Figure 7b).

**c) Mechanism of the interdecadal variability of eastward current**

To understand the mechanism that determines the interdecadal variability of the latitude $Y_b$ of the eastward current, we first look at the pattern of positive wind stress curl in the northwestern SCS and negative wind stress curl in the southeastern SCS in summer. To simply represent the pattern of summer wind stress curl in the SCS, we introduce another index, the latitude $W_b$, where the wind stress curl is zero along 113°E. Figure 8a shows the time series of the latitude $W_b$ derived from the summer wind stress curl for the period of 1960-2007. In general, the interdecadal signal and north-south shift of the zero wind stress curl line are similar to those of the eastward current. Before 1980, $W_b$ shifted to the south with time, from 13.5°N around 1965 to 9.3°N around 1979; this indicates that the region of positive wind stress curl in the northern SCS and that of negative one in the southern SCS were located more southward. Thus, the anomalous wind stress curls induced a southward migration of the northern cyclonic gyre and southern anticyclonic gyre. As a result, the eastward current associated with the two gyres moved southward. During 1980 to 1998, $W_b$ moved northward and reached the northernmost position in 1998; the eastward current shifted to the north correspondingly. After 1998, the eastward current moved to the south again with the southward shift of $W_b$. The trend rates of $W_b$ in three periods are also listed in Table 1.

As described in Section 3, to further investigate the mechanism of the interdecadal variability of the latitude $Y_b$ of the eastward current we also calculated SCSMI, and the time series of the SCSMI is shown in Figure 8b. The interdecadal signals of the SCSMI are consistent with that of $Y_b$. From 1965 to 1980, the SCSMI index increased from 0.02 to 0.06 $N/m^2$. After 1980, the index first declined and then increased again after 1998. The trend rates of the SCSMI in these three periods are listed in Table 1. The correlation coefficients between the SCSMI and $Y_b$ of three time series from the time-independent barotropic Sverdrup model, the time-dependent barotropic Sverdrup model and the time-dependent baroclinic Sverdrup model are -0.69, -0.70 and -0.72, respectively, all of them are significant at the 95% confidence level. The good correlation indicates the shift of the eastward current is strongly linked to the monsoon. When the SCSMI is strong (weak), the eastward flow is shifted southward (northward).

Therefore, the dynamic linkage between the SCS monsoon and the north-south position of the eastward current on interdecadal scale can be described as follows. Before 1980, the strengthening of the SCS monsoon gave rise to a weakened wind stress curl in the southern SCS and/or a strengthened wind stress curl in the northern SCS. The weakened (strengthened) wind stress curls implies a subdued (amplified) ocean gyre in the southern (northern) SCS, and the eastward jet between the two gyres moves southward through nonlinear processes (Wang et al., 2006). During 1980 to 1998, the monsoon index decreased, the anticyclonic gyre in the southern SCS intensified and/or the cyclonic gyre in the northern SCS weakened; therefore, the eastward jet moved northward. After 1998, the eastward jet moved southward again as the monsoon index was increased.

## 5. Summary and conclusion

In summer, SCS ocean circulation consists of a cyclonic gyre north of about 12°N and an anticyclonic gyre south of 12°N. Between these two gyres, there is an eastward current veering off central Vietnam. To the best of our knowledge, the interdecadal variability of the eastward current has not been examined. Our results show that the eastward jet moved southward, northward and southward during the periods of 1960-1979, 1980-1998 and 1999-2007, respectively.

We hypothesize that the interdecadal variability of the eastward current is strongly associated with the monsoon wind, which also shows interdecadal signals in wind stress curl pattern and wind stress strength. Firstly, the interdecadal shift of the zero wind stress curl line in the SCS is directly linked to the shift of the eastward current. In fact, the variations in wind stress curl change the position of the southern anticyclonic ocean gyre and northern cyclonic ocean gyre, inducing the shift of the eastward current between the two ocean gyres. Secondly, the competition of positive wind stress curl in the northern SCS and negative wind stress curl in the southern SCS is also an important source of interdecadal variability. As the SCS monsoon increased (decreased) during the periods of 1960-1979 and 1999-2007 (1980-1998), the anticyclonic gyre in the southern SCS weakened (strengthened) and the cyclonic gyre in the northern SCS were strengthened (weakened), and thus induced the southward (northward) migration of the eastward jet through nonlinear processes.

Our results also indicate that the eastward current in baroclinic streamfunction is located about 0-6.6$^{o}$ (mean value is 1.7$^{o}$) farther southward than that from the barotropic streamfunction, suggesting that the meridional shift of the eastward current is depth dependent.

The SCS monsoon has a robust interdecadal variability, but the mechanisms for the interdecadal monsoon change remains to be explained (Wang et al., 2009). The present work shows the interdecadal variability of the monsoon is a major cause of the interdecadal variability of the eastward jet in the SCS. However, the influence of the interdecadal variability of the eastward jet on the SCS sea surface temperature and chlorophyll signature remains a challenging issue.

**Acknowledgement:** This study was supported by the National Basic Research Program (2007CB816003) and the National Natural Science Foundation of China (Grant #: 40976017, 40730843 and 40876004). We also thank Dr. Cai Shuqun who kindly provided the code for calculating the Rossby wave speed, and Mr. Ling Zheng who helped preparing the manuscript. Helpful comments from the three anonymous reviewers are greatly appreciated.

**Reference:**


Bayler, E. J., and Z. Liu, 2008: Basin-scale wind-forced dynamics of the seasonal southern South China Sea gyre, J. Geophys. Res., 113, C07014, doi:10.1029/2007JC004519.

Carton, J. A., and B. S. Giese, 2008: A reanalysis of ocean climate using Simple Ocean Data Assimilation (SODA). *Mon. Wea. Rev*., **136**, 2999-3017.

Cai, S.Q., X. M. Long, R. H. Wu, and S. G. Wang, 2008: Geographical and monthly variability of the first baroclinic Rossby radius of deformation in the South China Sea. *J. Mar. Sys*., **74**, 711–720.

Fang, W. D., G. H. Fang, P. Shi, Q. Z. Huang, and Q. Xie, 2002: Seasonal structures of upper layer circulation in the southern South China Sea from in situ observations. *J. Geophys. Res*., **107** (C11), 3202, doi:10.1029/2002JC001343.

Gan, J., and T. Qu, 2008: Coastal jet separation and associated flow variability in the Southwest South China sea. *Deep Sea Res. I*, 55, 1–19.

Hu, Z. Z., 1997: Interdecadal variability of summer climate over East Asia and its association with 500hpa height and global sea surface temperature. *J. Geophys. Res*., **102**, 19403-19412.

Huang, R. X., and Q. Y. Liu, 2010: Meridional circulation in the western coastal zone: I. Variability of off-shore thermocline depth and western boundary current transport on interannual and decadal time scales. Submitted to *J. Phys. Oceanogr*.

Kuo, N. J., Q. A. Zheng, and C. R. Ho, 2000: Satellite observation of upwelling along the western coast of the South China Sea. *Remote Sens.Environ*., **74**, 463– 470.

Liu, K.-K., S.-Y. Chao, P.-T. Shaw, G. C. Gong, C. C. Chen, and T. Y. Tang, 2002: Monsoon forced chlorophyll distribution and primary productivity in the South China Sea: Observations and a numerical study. *Deep Sea Res*., Part I, **49**, 1387–1412.

Liu, Z. Y., H. J. Yang, and Q. Y. Liu, 2001: Regional dynamics of seasonal variability in the South China Sea. *J. Phys. Oceanogr*., **31**, 272–284.

Metzger, E. J., and H. Hurlburt, 1996: Coupled dynamics of the South China Sea, the Sulu Sea, and the Pacific Ocean. *J. Geophys. Res*., **101**, 12,331– 12,352.

Qiu, B. and R. Lukas, 1996: Seasonal and interannual variability of the North Equatorial Current, the Mindanao Current and the Kuroshio along the Pacific western boundary. J. Geophys. Res., 101 12,315-12,330.

Wang B., F. Huang, Z. Wu, J. Yang, Fu X., and K. Kikuchi, 2009: Multi-scale climate variability of the South China Sea monsoon: A review. *Dynamics of Atmospheres and Oceans*, **47** (1-3), 15-37.

Wang, G., 2004: Discussion on the movement of mesoscale eddies in the South China Sea (in Chinese), Ph.D. dissertation, Sch. of Phys. Oceanogr., Ocean Univ. of China, Qingdao, China. 96PP.

Wang, G., D. Chen and J. Su, 2006: Generation and Life Cycle of the Dipole in South China Sea Summer Circulation. *J. Geophys. Res*., **111**, C06002, doi: 10.1029/ 2005JC003314.

Xie, S. P., Q. Xie, D. X. Wang, and W. T. Liu, 2003: Summer up welling in the South

China Sea and its role in regional climate variations. *J. Geophys. Res*., **108** (C8), 3261, doi:10.1029/2003JC001867.

Xu, X. Z., Z. Qiu, and H. C. Chen, 1982: The general descriptions of the horizontal circulation in the South China Sea, in Proceedings of the 1980 Symposium on Hydrometeorology (in Chinese). *Chin. Soc. of Oceanol. and Limnol.*, Sci. Press, Beijing, 137–145.

Table 1. The trend rates in three periods for the South China Sea monsoon index (SCSMI), the position of zero line of wind stress curl along 113°E ($W_b$), the position of eastward current($T_b$) from Simple Ocean Data Assimilation (SODA) dataset and the position of eastward current ($Y_b$) derived from three types of Sverdrup streamfunction: the time-independent barotropic model (TIBT), the time-dependent barotropic model (TDBT) and the time-dependent baroclinic model (TDBC). The units for the SCSMI, $W_b$ and $Y_b$ are $N/m^2$ per year, °N per year and °N per year, respectively.

| Models | 1960-1979 | 1979-1998 | 1998-2008 |
|---|---|---|---|
| SODA | -0.080 | 0.062 | -0.050 |
| TIBT | -0.074 | 0.164 | -0.460 |
| TDBT | -0.125 | 0.191 | -0.338 |
| TDBC | -0.175 | 0.212 | -0.503 |
| $W_B$ | -0.0288 | 0.0795 | -0.2925 |
| SCSMI | 0.0011 | -0.0008 | 0.0052 |

**Figure 1**. Climatological summer mean isotherm depth (m) of 20°C from SODA. Shaded values indicate the depth larger than 105m. The dot denotes the summer mean latitude of $T_b$ where the depth of 20℃ is 100m along the 113°E section.

**Figure 2**. Climatological summer mean zonal velocity (m/s) across 7°N-15°N along 112.75°E taken from SODA. Positive values indicate eastward flow.

**Figure 3.** (a) Summer mean ERA-40 wind stress (vectors, N/m2) and wind stress curl (contours, 10-6 N/m3). The dot denotes the latitude of summer mean zero wind stress curl line. (b) Summer mean Sverdrup transport (Sv) derived from the time-independent barotropic Sverdrup model. The cyan line in (b) is the position for the eastward current derived from the model. The dot denotes $Y_b$ of eastward current in the summer mean streamfunction. In (a) and (b), the positive values are shaded and negative values are contoured. The thick dashed line is for the 200m isobaths.

**Figure 4**. (a) Summer mean Sverdrup streamfunction (Sv) derived from the time-dependent barotropic Sverdrup model. (b) Summer mean Sverdrup streamfunction (Sv) derived from the time-dependent baroclinic Sverdrup model. The green lines in (a) and (b) are for the position of the eastward current derived from the time-dependent barotropic Sverdrup model. The red line in (b) is for the position of

the eastward current derived from the time-dependent baroclinic Sverdrup model. The positive values are shaded and negative values are contoured.

**Figure 5.** Time series of the eastward current latitude derived from SODA. The black line is the original latitude of eastward current from SODA data, the blue line is the latitude with the 15-year low passed Butterworth filter. The green straight lines are the fit lines in three periods for orginal one.

**Figure 6**. a1,a2 and a3 are summer mean Sverdrup transport (Sv) derived from the time-independent barotropic Sverdrup model over the period of 1960-1979,1980-1998 and 1999-2008 respectively; b1,b2,and b3 are as a1,a2,a3 but for time-dependent barotropic Sverdrup model; c1,c2 and c3 are for time-dependent baroclinic Sverdrup model.

**Figure 7.** (a) Time series of the eastward current latitude derived from time-independent barotropic Sverdrup model (TIBT), time-dependent barotropic Sverdrup model (TDBT) and time-dependent baroclinic Sverdrup model (TDBC). The green straight lines are the fit lines in three periods for TDBT. (b) The difference between TDBT and TDBC (TDBT minus TDBC). The positive value denotes that TDBT is more northward than TDBC.

**Figure 8.** (a) Time series of the latitude of the summer zero wind stress curl line ($W_b$) along 113$^o$E. (b) The South China Sea monsoon index (SCSMI) during summer. The straight lines are the fit lines in three periods.

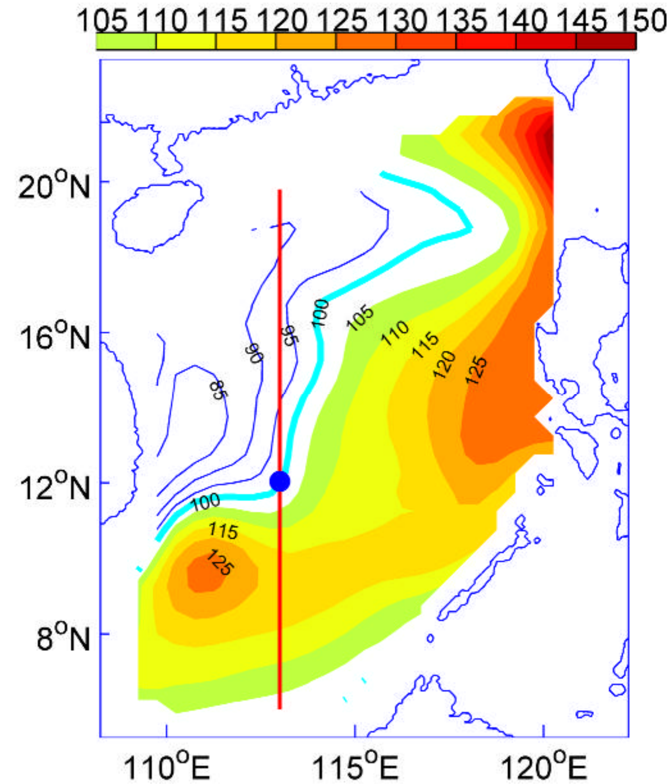


**Figure 1**. Climatological summer mean isotherm depth (m) of 20°C from SODA. Shaded values indicate the depth larger than 105m. The dot denotes the summer mean latitude of $T_b$ where the depth of 20℃ is 100m along the 113°E section.

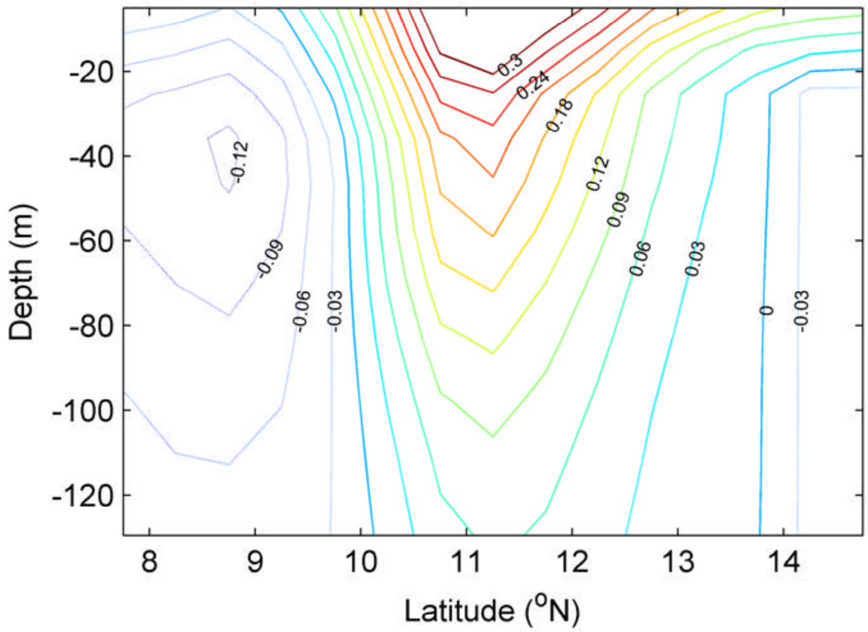


**Figure 2**. Climatological summer mean zonal velocity (m/s) across 7°N-15°N along 112.75°E taken from SODA. Positive values indicate eastward flow.

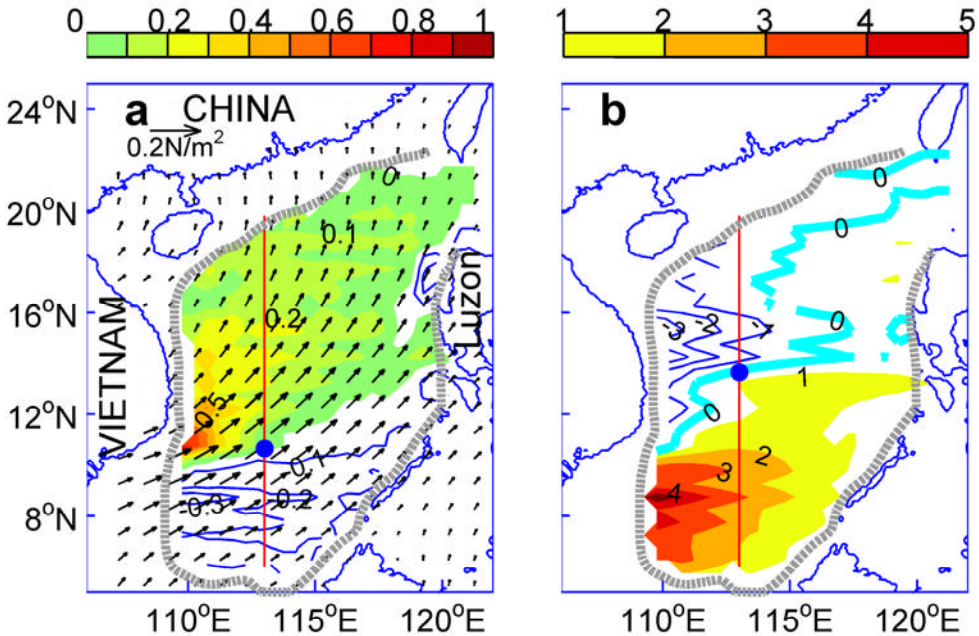


**Figure 3**. (a) Summer mean ERA-40 wind stress (vectors, N/m$^2$) and wind stress curl (contours, $10^{-6}$ N/m$^3$). The dot denotes the latitude of summer mean zero wind stress curl line. (b) Summer mean Sverdrup transport (Sv) derived from the time-independent barotropic Sverdrup model. The cyan line in (b) is the position for the eastward current derived from the model. The dot denotes $Y_b$ of eastward current in the summer mean streamfunction. In (a) and (b), the positive values are shaded and negative values are contoured. The thick dashed line is for the 200m isobaths.

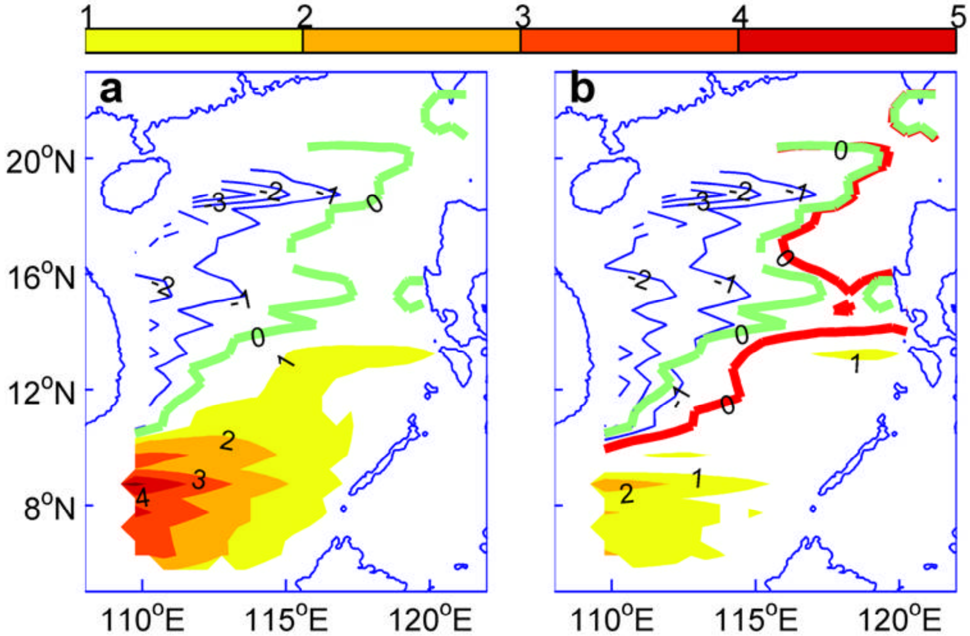


**Figure 4**. (a) Summer mean Sverdrup streamfunction (Sv) derived from the time-dependent barotropic Sverdrup model. (b) Summer mean Sverdrup streamfunction (Sv) derived from the time-dependent baroclinic Sverdrup model. The green lines in (a) and (b) are for the position of the eastward current derived from the time-dependent barotropic Sverdrup model. The red line in (b) is for the position of the eastward current derived from the time-dependent baroclinic Sverdrup model. The positive values are shaded and negative values are contoured.

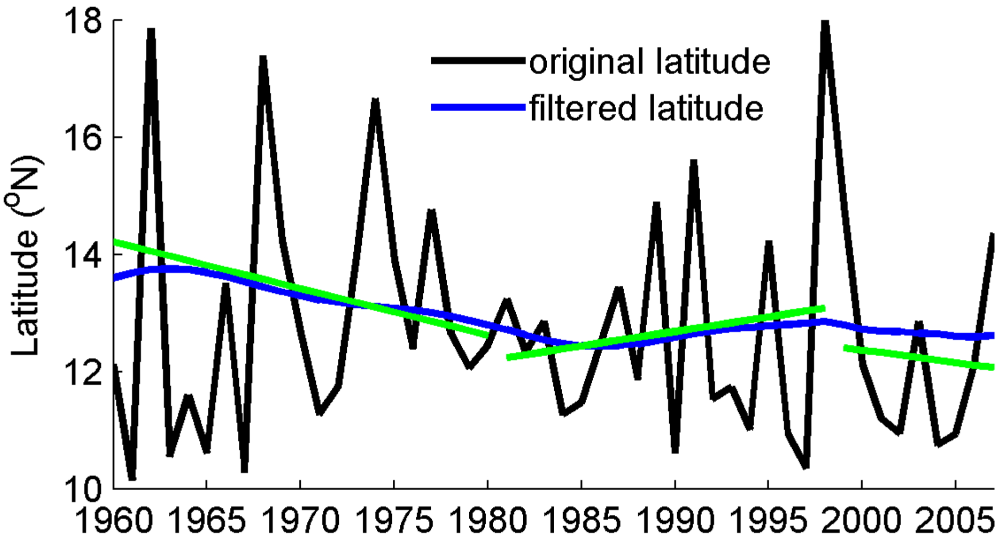


**Figure 5.** Time series of the eastward current latitude derived from SODA. The black line is the original latitude of eastward current from SODA data, and the blue line is the latitude with the 15-year low passed Butterworth filter. The green straight lines are the linear fit lines in three periods from the orginal one.

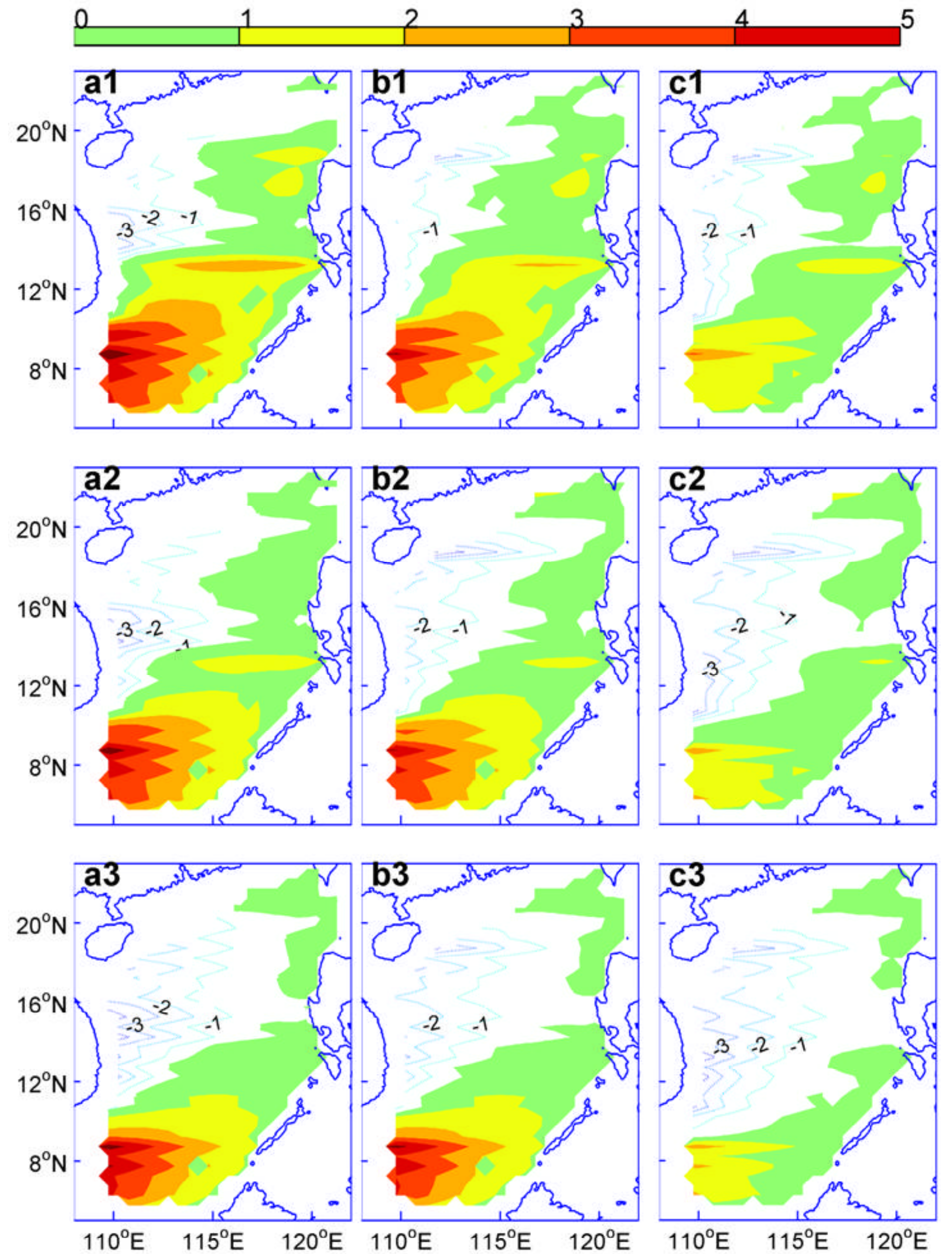


**Figure 6**. a1,a2 and a3 are summer mean Sverdrup transport (Sv) derived from the time-independent barotropic Sverdrup model over the period of 1960-1979,1980-1998 and 1998-2008 respectively; b1,b2,and b3 are as a1,a2,a3 but for time-dependent barotropic Sverdrup model; c1,c2 and c3 are for time-dependent baroclinic Sverdrup model.

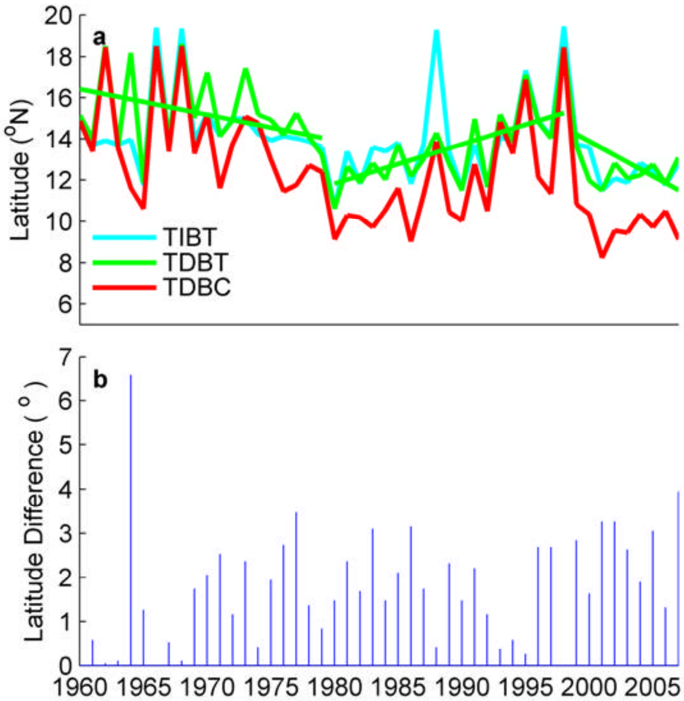


**Figure 7.** (a) Time series of the eastward current latitude derived from time-independent barotropic Sverdrup model (TIBT), time-dependent barotropic Sverdrup model (TDBT) and time-dependent baroclinic Sverdrup model (TDBC). The green straight lines are the fit lines in three periods for TDBT. (b) The difference between TDBT and TDBC (TDBT minus TDBC). The positive value denotes that TDBT is more northward than TDBC.

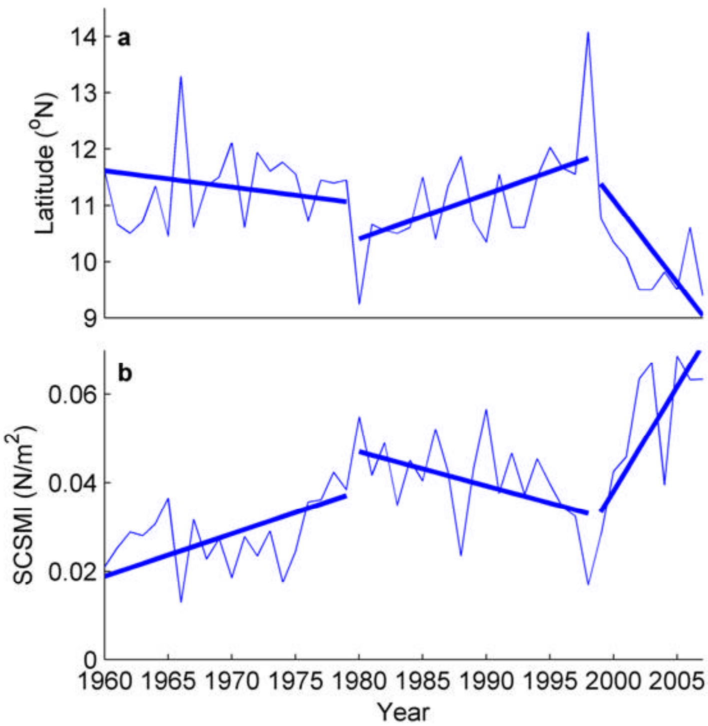


**Figure 8.** (a) Time series of the latitude of the summer zero wind stress curl line ($W_b$) along 113°E. (b) The South China Sea monsoon index (SCSMI) during summer. The straight lines are the fit lines in three periods.